Rapid Communications

Effect of elastic walls on suspension flow

Marco Edoardo Rosti, Mehdi Niazi Ardekani, and Luca Brandt
Linné Flow Centre and SeRC (Swedish e-Science Research Centre), KTH Mechanics, SE-100 44 Stockholm, Sweden

(Received 4 November 2018; revised manuscript received 2 April 2019; published 21 June 2019)

We study suspensions of rigid particles in a plane Couette flow with deformable elastic walls. We find that, in the limit of vanishing inertia, the elastic walls induce shear thinning of the suspension flow such that the effective viscosity decreases as the wall deformability increases. This shear-thinning behavior originates from the interactions between rigid particles, soft walls, and carrier fluids; an asymmetric wall deformation induces a net lift force acting on the particles which therefore migrate towards the bulk of the channel. Based on our observations, we provide a closure for the suspension viscosity which can be used to model the rheology of suspensions with arbitrary volume fraction in elastic channels.

DOI: 10.1103/PhysRevFluids.4.062301

Understanding how elastic structures interact with fluid flows is a problem attracting a great deal of attention in different fields of science and technology, ranging from biological applications [1–5] to energy harvesting [6,7]. In this context we consider a fluid-structure interaction problem particularly relevant to understand biological flows: We study the rheology of suspensions in the presence of walls which are allowed to deform elastically.

The study of rheology is motivated by the many fluids in nature and industrial applications which exhibit a non-Newtonian behavior, i.e., a nonlinear relation between the shear stress and the shear rate, such as shear thinning, shear thickening, yield stress, thixotropy, shear banding, and viscoelastic behaviors. The relation between these macroscopic behaviors and the microstructure is often studied assuming suspensions of objects in a Newtonian solvent with dynamic viscosity μ_0 and density ρ. In the simplest case of suspensions of rigid spheres in a Newtonian fluid, Einstein [8] showed in his pioneering work that in the limit of vanishing inertia and for dilute suspensions (i.e., $\Phi \to 0$), the relative increase in effective viscosity μ_e is a linear function of the particle volume fraction Φ. However, at present there is no theory that allows us to calculate μ_e for any given Φ, thus different empirical formulas have been proposed to provide a good description for the existing experimental and numerical results [9–11]. Among those, we consider here the Eilers formula [12,13],

$$\frac{\mu}{\mu_0} = \left[1 + B\frac{\Phi}{1 - \Phi/\Phi_m}\right]^2, \tag{1}$$

which well fits the experimental and numerical data [11,14] for both low and high values of Φ, up to about 0.6. In the expression above, Φ_m is the geometrical maximum packing fraction and B a constant; fits to the data are usually obtained for $\Phi_m = 0.58$–0.63 and $B = 1.25$–1.7.

In this Rapid Communication we add a further complexity to this problem, one that is particularly relevant to understand the rheology of biological flows: We allow the walls to deform elastically. The problem of a single object interacting with a soft wall has been the object of several recent works [15–22]; on the other hand, here we focus on particle suspensions interacting with soft walls. In particular, we model the walls as two viscoelastic layers with an elastic shear-modulus

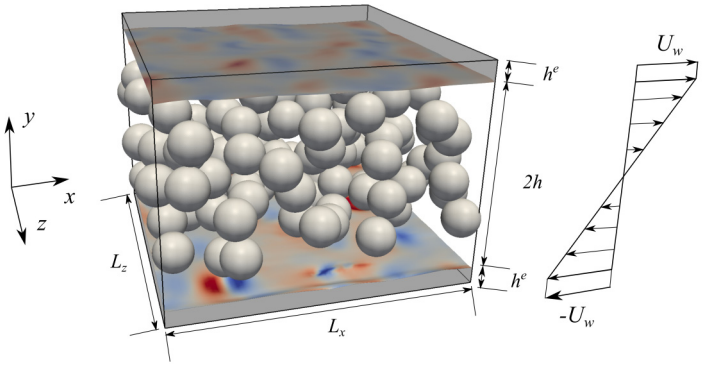

FIG. 1. Visualization of the particle suspension in a Couette flow with elastic walls, with a sketch of the relevant geometrical parameters.

G and viscosity μ_m. Thus, we introduce two dimensionless parameters in the problem: the capillary number $\mathrm{Ca} \equiv \mu_0 \dot{\gamma}/G$ and the solid to fluid viscosity ratio $K \equiv \mu_m/\mu_0$, the latter fixed to 1 for simplicity. We aim to describe the nonlinear effects of the wall elasticity on the rheology of a suspension. Furthermore, we will provide a simple approach that is able to accurately model the presence of deformable walls, without the necessity to solve the complex nonlinear interactions between the multiphase flow and the structure dynamics.

To address this problem, we perform direct numerical simulations of suspensions of rigid spheres, simulated by an immersed boundary method [23], flowing in a plane channel Couette flow. Two viscoelastic layers are attached to the moving rigid walls, simulated with a pseudovolume of fluid approach [24] (see Fig. 1 for a sketch of the geometry considered [25]). We cover a wide range of volume fractions Φ (up to 30%) and capillary numbers Ca (up to 8) and calculate the effective viscosity of the suspension $\mu_e = \mathcal{F}(\Phi, \mathrm{Ca})$. This is displayed in Fig. 2 for different volume fractions Φ and for various levels of wall elasticity, i.e., for various capillary numbers Ca. Also, three different thicknesses h^e of the elastic walls are considered: $0.5R$, R, and $1.5R$. We observe that the suspension viscosity increases with the volume fraction Φ but decreases with the wall deformability (increasing

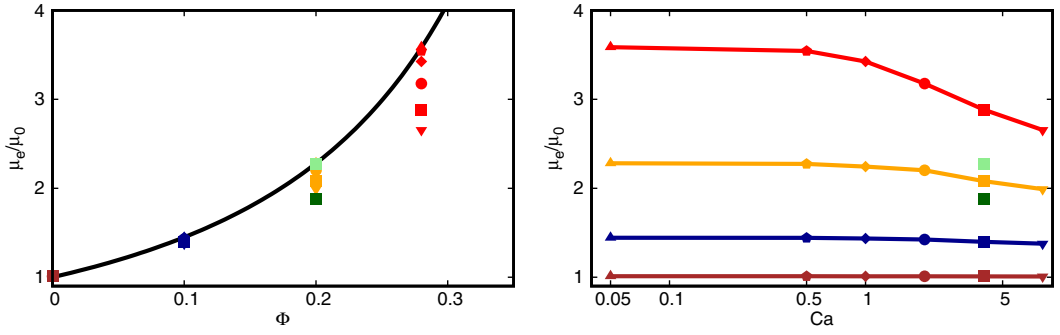

FIG. 2. Effective viscosity of the suspension μ_e as a function of the volume fraction Φ (left) and capillary number Ca (right). The effective viscosity is normalized with the fluid viscosity μ_0. The brown, blue, orange, and red colors are used for volume fractions Φ equal to 0.0016, 0.1, 0.2, and 0.29, while the symbols △, ⬠, ◇, ⨀, □, and ▽ for capillary numbers Ca equal to 0.05, 0.5, 1, 2, 4, and 8. All the previous symbols and colors are used for an elastic layer of thickness $h^e = R$; the light and dark green squares represent the results for $\Phi = 0.2$, $\mathrm{Ca} = 4$, and $h^e = 0.5R$ and $1.5R$, respectively. The black line in the left panel is the Eilers formula, Eq. (1), with $\Phi_m = 0.6$ and $B = 1.7$.

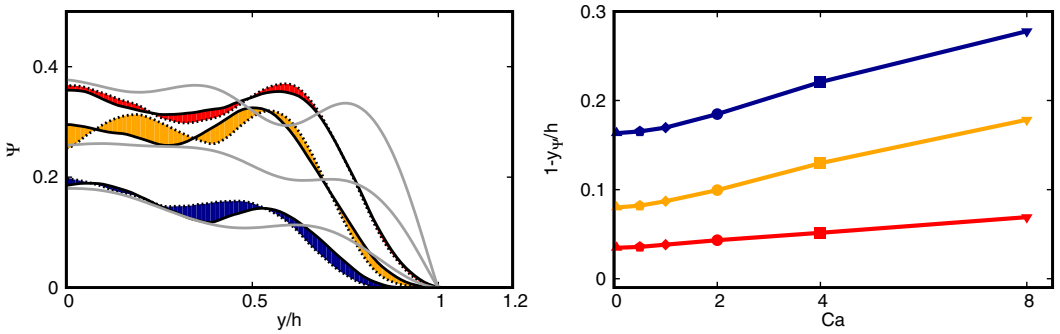

FIG. 3. Left: Mean particle concentration Ψ as a function of y. The shaded areas represent the variation due to the capillary number Ca, with the black solid and dashed lines representing the lowest and highest values of Ca; the gray solid lines are the data for rigid walls. Right: Distance from the wall $h - y$ at which the mean particle concentration is equal to 0.01 of the nominal value as a function of the capillary number Ca.

capillary number). The effect of the wall deformability is more pronounced as the volume fraction increases, where we observe larger differences from the reference case (rigid walls), indicated by the Eilers fit in the figure (solid black line). In particular, we find a reduction of up to 25% in the effective viscosity at $\Phi \approx 30\%$ for the largest capillary number considered in this study. Note that the reduction of the suspension viscosity with the capillary number can be interpreted as a shear-thinning rheological behavior of the system (see Fig. 2) where the effective viscosity μ_e is shown as a function of Ca. Interestingly, similar behavior was observed in Ref. [27] for suspensions of deformable particles. It is worth noticing that the presence of the elastic wall has no effect on the fluid rheology in the absence of particles, i.e., $\mu_e = \mu_0$ when $\Phi = 0$. Thus, the observed shear thinning is the result of the interaction of the elastic walls and the particles. This behavior is affected by the thickness of the elastic layer h^e: When the size of the layer is increased, the effect on the suspension is enhanced and the effective viscosity further reduces. To understand the mechanism that generates the shear-thinning behavior of the suspension, we study the mean particle concentration $\Psi(y)$ across the channel, shown in the left panel of Fig. 3. The particle concentration Ψ is null inside the elastic layer ($y \geqslant h$), rapidly grows in the near wall region ($h/2 \lesssim y \lesssim h$), and finally reaches an approximately uniform value in the middle of the channel ($h \lesssim h/2$). Unlike the case of rigid walls (gray line), on average there are no particles in contact with the deformable wall as these are lifted towards the channel center. As the total volume fraction Φ increases, the concentration distribution grows faster close to the wall and reaches higher values at the bulk of the channel to ensure the imposed total volume fraction Φ. The effect of the wall elasticity is shown by the shaded colored areas in the graph: As Ca increases, the particles are displaced farther away from the wall and concentrate more in the bulk of the channel. This effect is present for all the volume fractions Φ and capillary numbers Ca that we studied, but is more evident at low volume fractions than at high ones due to the larger available space for the particles to migrate. Note that, despite this, the effect on the effective viscosity of the suspension increases with the volume fraction, as shown in Fig. 2. The mean displacement of the particles from the wall is quantified in the right panel of Fig. 3, where the wall-normal distance ($h - y$) at which the concentration Ψ is equal to 1% of the nominal value is reported as a function of the capillary number Ca. The wall-normal distance where $\Psi = 1\%$ increases for all the volume fractions with the capillary number Ca, i.e., as the wall becomes more deformable, and decreases for increasing total volume fraction Φ. The displacement of the particles from the walls to the center of the channel can be related to the nonzero wall-normal velocity fluctuations v' at the elastic walls ($y = h$), although the mean wall-normal velocity is zero for incompressible materials. These fluctuations are shown in Fig. 4, where v' is reported as a function of the capillary number Ca for all the volume fractions Φ considered. We observe that

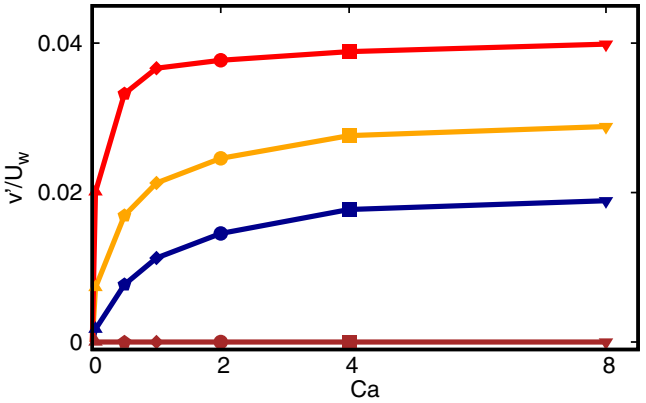

FIG. 4. Root mean square of the wall-normal velocity fluctuations v' at the interface between the fluid and deformable wall $y = h$ as a function of the capillary number Ca.

v' grows from zero as the capillary number is increased, i.e., the wall is allowed to deform; the fluctuation growth rate is high for low capillary numbers before we observe a tendency to saturate. Also, the decrease of the growth rate at high capillary numbers is faster for high volume fractions, in accordance with what already observed in Fig. 3. The wall-normal velocity fluctuations are induced by the deformation of the walls due to the interaction with the rigid particles, as sketched in Fig. 5. A particle approaching the elastic wall deforms it, generating a wall-normal flow; in addition, the particle moves along the wall due to the applied shear. The combination of these two effects induces an asymmetric wall deformation which leads to the generation of a net lift force acting on the particle, which therefore migrates away from the wall. These results are consistent with and confirm previous theoretical works [16,18] which considered the deformations induced by a single rigid sphere translating parallel to a soft wall in a viscous fluid; in these previous studies, lubrication theory is shown to predict a lift force acting on the object, as observed experimentally [17].

Finally, we propose a model to easily include the effect of the elastic walls in the rheological description of suspensions. As mentioned above, μ_e is in general a nonlinear function of the total volume fraction Φ and the capillary number of the walls Ca, i.e., $\mu_e = \mathcal{F}(\Phi, \mathrm{Ca})$. Below, we show that μ_e can be written as a function of a single variable Φ_e, i.e., $\mu_e = \mathcal{G}(\Phi_e)$. Also, we will demonstrate that the nonlinear function $\mathcal{G}$ can be properly described by the Eilers fit reported in Eq. (1), similarly to the standard case of flow over rigid walls. The effective volume fraction Φ_e takes into account the fact that the particles feel a reduced confinement effect due to the wall flexibility: Indeed, they can move beyond $y = h$ by inducing wall deformations. Thus, we introduce a reduced effective volume fraction, obtained by increasing the total volume available to the particles by a

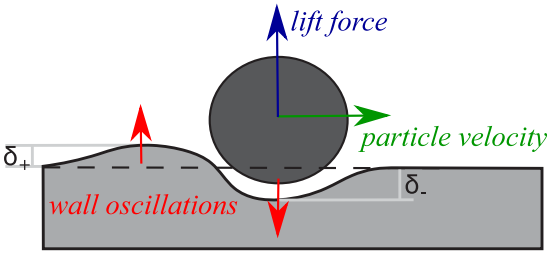

FIG. 5. Sketch of the mechanism of the lift generation induced by the interaction of a moving sphere and a rigid particle.

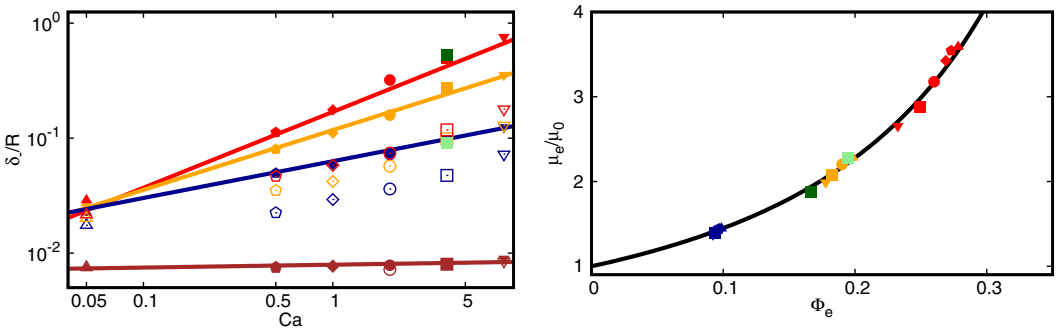

FIG. 6. Left: Mean wall deformations $\delta_\pm$ as a function of the capillary number Ca. The solid and open points are the negative δ_- and positive δ_+ wall deformations, respectively, while the solid lines are fits to our data in the form of Eq. (2). Right: Normalized effective viscosity μ_e as a function of the effective volume fraction Φ_e computed from Eq. (3). The black solid line is the Eilers formula reported in Eq. (1).

layer of thickness δ_-, which is the amount of the penetration of the particles into the walls, or alternatively, the amplitude of the average negative wall deformation. We plot in the left panel of Fig. 6 the normalized amplitude of wall deformation δ_-, which grows with both the wall elasticity Ca and the volume fraction Φ. A simple fit of our data (shown with the solid lines in the plot) provides the following expression for δ_- as a function of the volume fraction Φ, the capillary number Ca, and the elastic layer thickness h^e,

$$\frac{\delta_-}{R} \approx \Phi^{c_1} \mathrm{Ca}^{c_2} \left(\frac{h^e}{R}\right)^{c_3}, \tag{2}$$

where c_i are fitting coefficients, $c_1 \approx 0.9$, $c_3 \approx 1.5$, and $c_2 \approx 0.32$ for $\Phi = 0.1$, 0.52 for $\Phi = 0.2$, and 0.66 for $\Phi = 0.29$. Note that Fig. 6 reports also δ_+, the amplitude of the positive wall deformation, which is always smaller than δ_- due to the aforementioned symmetry breaking at the deformable wall interface. Once δ_- is known, one can compute the effective volume fraction as

$$\Phi_e = \mathcal{N} \frac{\frac{4}{3}\pi R^3}{\mathcal{V}^e_{\mathrm{tot}}}, \tag{3}$$

where $\mathcal{V}^e_{\mathrm{tot}}$ is the sum of the total volume originally available to the particles $\mathcal{V}_{\mathrm{tot}} = 2h\,L_x\,L_z$ and the increase due to the wall elasticity $\mathcal{V}^e = \delta\,L_x\,L_z$, i.e., $\mathcal{V}^e_{\mathrm{tot}} = \mathcal{V}_{\mathrm{tot}} + \mathcal{V}^e = 2(h + \delta_-)\,L_x\,L_z$. The right panel in Fig. 6 shows again the effective viscosity μ_e now as a function of the effective volume fraction Φ_e. We observe that all the cases at different volume fractions Φ, capillary numbers Ca, and wall thickness h^e collapse onto a single curve, which is well described by the Eilers formula. Thus, by using Eqs. (2) and (1) we are able to effectively predict the suspension effective viscosity μ_e in the presence of elastic walls, once the volume fraction Φ, the capillary number Ca, and the thickness of the elastic layers h^e are known. Also, we explain the largest variations of the effective viscosity μ_e at higher volume fractions by the large sensitivity of μ_e to variations of Φ at higher concentrations (slope of the Eilers curve).

In conclusion, we have explored the rheological behavior of a suspension of rigid particles in an elastic channel, for a wide range of solid volume fractions and wall elasticities. The main results of our analysis are the identification of a shear-thinning behavior of the suspension induced by the interaction of the elastic walls and the rigid particles, and its explanation in terms of a lift force acting on the particles which induces their migration towards the bulk of the channel. The lift force mechanism is robust enough to be effective also in relatively dense suspensions, whose behavior is usually mainly determined by interparticle interactions. Based on our observations and a simple mechanical model, we also provide a closure to effectively predict the rheological properties of

suspensions in the presence of elastic walls. Our results extend to deformable walls the idea of using simple empirical fits, originally valid for inertialess suspensions of rigid spheres, such as the Eilers formula, to predict the rheology of suspensions with additional complexity embedded in the definition of an effective volume fraction, as previously done in Refs. [29], [28], and [27] for the cases of inertial effects, particle shapes, and deformability, respectively. The applicability of this scaling confirms that viscous dissipation is still the dominant mechanism at work in these flows.

The authors were supported by the ERC 2013-CoG-616186 TRITOS and by the VR 2014-5001 and acknowledge the computer time provided by SNIC (Swedish National Infrastructure for Computing).

[1] M. Abkarian, C. Lartigue, and A. Viallat, Tank Treading and Unbinding of Deformable Vesicles in Shear flow: Determination of the Lift Force, Phys. Rev. Lett. **88**, 068103 (2002).
[2] F. E. Fish and G. V. Lauder, Passive and active flow control by swimming fishes and mammals, Annu. Rev. Fluid Mech. **38**, 193 (2006).
[3] J. B. Freund, Numerical simulation of flowing blood cells, Annu. Rev. Fluid Mech. **46**, 67 (2014).
[4] G. W. Greene, X. Banquy, D. W. Lee, D. D. Lowrey, J. Yu, and J. N. Israelachvili, Adaptive mechanically controlled lubrication mechanism found in articular joints, Proc. Natl. Acad. Sci. USA **108**, 5255 (2011).
[5] A. J. Grodzinsky, H. Lipshitz, and M. J. Glimcher, Electromechanical properties of articular cartilage during compression and stress relaxation, Nature (London) **275**, 448 (1978).
[6] C. Boragno, R. Festa, and A. Mazzino, Elastically bounded flapping wing for energy harvesting, Appl. Phys. Lett. **100**, 253906 (2012).
[7] W. McKinney and J. DeLaurier, Wingmill: An oscillating-wing windmill, J. Energy **5**, 109 (1981).
[8] A. Einstein, *Investigations on the Theory of the Brownian Movement* (Dover, New York, 1956).
[9] F. Ferrini, D. Ercolani, B. De Cindio, L. Nicodemo, L. Nicolais, and S. Ranaudo, Shear viscosity of settling suspensions, Rheol. Acta **18**, 289 (1979).
[10] P. M. Kulkarni and J. F. Morris, Suspension properties at finite Reynolds number from simulated shear flow, Phys. Fluids **20**, 040602 (2008).
[11] A. Singh and P. R. Nott, Experimental measurements of the normal stresses in sheared Stokesian suspensions, J. Fluid Mech. **490**, 293 (2003).
[12] J. Mewis and N. J. Wagner, *Colloidal Suspension Rheology* (Cambridge University Press, Cambridge, UK, 2012).
[13] J. J. Stickel and R. L. Powell, Fluid mechanics and rheology of dense suspensions, Annu. Rev. Fluid Mech. **37**, 129 (2005).
[14] I. E. Zarraga, D. A. Hill, and D. T. Leighton, Jr., The characterization of the total stress of concentrated suspensions of noncolloidal spheres in Newtonian fluids, J. Rheol. **44**, 185 (2000).
[15] M. Mani, A. Gopinath, and L. Mahadevan, How Things Get Stuck: Kinetics, Elastohydrodynamics, and Soft Adhesion, Phys. Rev. Lett. **108**, 226104 (2012).
[16] B. Rallabandi, B. Saintyves, T. Jules, T. Salez, C. Schoenecker, L. Mahadevan, and H. A. Stone, Rotation of an immersed cylinder sliding near a thin elastic coating, Phys. Rev. Fluids **2**, 074102 (2017).
[17] B. Saintyves, T. Jules, T. Salez, and L. Mahadevan, Self-sustained lift and low friction via soft lubrication, Proc. Natl. Acad. Sci. USA **113**, 5847 (2016).
[18] T. Salez and L. Mahadevan, Elastohydrodynamics of a sliding, spinning and sedimenting cylinder near a soft wall, J. Fluid Mech. **779**, 181 (2015).
[19] J. M. Skotheim and L. Mahadevan, Soft Lubrication, Phys. Rev. Lett. **92**, 245509 (2004).
[20] B. Rallabandi, N. Oppenheimer, M. Y. B. Zion, and H. A. Stone, Membrane-induced hydroelastic migration of a particle surfing its own wave, Nat. Phys. **14**, 1211 (2018).
[21] J. Beaucourt, T. Biben, and C. Misbah, Optimal lift force on vesicles near a compressible substrate, Europhys. Lett. **67**, 676 (2004).

[22] H. S. Davies, D. Debarre, N. El. Amri, C. Verdier, R. P. Richter, and L. Bureau, Elastohydrodynamic Lift at a Soft Wall, Phys. Rev. Lett. **120**, 198001 (2018).

[23] D. Izbassarov, M. E. Rosti, M. N. Ardekani, M. Sarabian, S. Hormozi, L. Brandt, and O. Tammisola, Computational modeling of multiphase viscoelastic and elastoviscoplastic flows, Int. J. Numer. Methods Fluids **88**, 521 (2018).

[24] M. E. Rosti and L. Brandt, Numerical simulation of turbulent channel flow over a viscous hyper-elastic wall, J. Fluid Mech. **830**, 708 (2017).

[25] The equations of motion are solved using the second-order finite-difference scheme in space and the third-order Runge-Kutta scheme in time. We use a Cartesian uniform mesh in a rectangular box of size $16R \times (10R + 2h^e) \times 16R$, discretized with 16 grid points per particle radius R, where h^e is the elastic layer thickness. Periodic boundary conditions are imposed in the streamwise x and spanwise z directions and no-slip conditions at the rigid and elastic walls located at $y = \pm(h + h^e)$ and $y = \pm h$, respectively, with y the wall-normal direction. The rigid walls move in opposite directions with constant streamwise velocity $\pm U_w$. See the Supplemental Material for further details on the numerical method [26].

[26] See Supplemental Material at http://link.aps.org/supplemental/10.1103/PhysRevFluids.4.062301 for further details on the numerical method, Refs. [30–36].

[27] M. E. Rosti, L. Brandt, and D. Mitra, Rheology of suspensions of viscoelastic spheres: Deformability as an effective volume fraction, Phys. Rev. Fluids **3**, 012301(R) (2018).

[28] S. Mueller, E. W. Llewellin, and H. M. Mader, The rheology of suspensions of solid particles, Proc. R. Soc. London, Ser. A **466**, 1201 (2010).

[29] F. Picano, W. P. Breugem, D. Mitra, and L. Brandt, Shear Thickening in Non-Brownian Suspensions: An Excluded Volume Effect, Phys. Rev. Lett. **111**, 098302 (2013).

[30] I. A. Bolotnov, K. E. Jansen, D. A. Drew, A. A. Oberai, R. T. Lahey, Jr., and M. Z. Podowski, Detached direct numerical simulations of turbulent two-phase bubbly channel flow, Int. J. Multiphase Flow **37**, 647 (2011).

[31] J. Bonet and R. D. Wood, *Nonlinear Continuum Mechanics for Finite Element Analysis* (Cambridge University Press, Cambridge, UK, 1997).

[32] P. Costa, B. J. Boersma, J. Westerweel, and W. P. Breugem, Collision model for fully resolved simulations of flows laden with finite-size particles, Phys. Rev. E **92**, 053012 (2015).

[33] D. J. Jeffrey, Low-Reynolds-number flow between converging spheres, Mathematika **29**, 58 (1982).

[34] J. Kim and P. Moin, Application of a fractional-step method to incompressible Navier-Stokes equations, J. Comput. Phys. **59**, 308 (1985).

[35] T. Min, J. Y. Yoo, and H. Choi, Effect of spatial discretization schemes on numerical solutions of viscoelastic fluid flows, J. Non-Newtonian Fluid Mech. **100**, 27 (2001).

[36] G. Tryggvason, M. Sussman, and M. Y. Hussaini, Immersed boundary methods for fluid interfaces, in *Computational Methods for Multiphase Flow*, edited by A. Prosperetti and G. Tryggvason (Cambridge University Press, Cambridge, UK, 2007), pp. 37–77.